View metadata, citation and similar papers at core.ac.uk

brought to you by CORE

provided by Arrow@dit

Technological University Dublin

ARROW@TU Dublin

Articles

NanoLab

2019

Numerically Modelling Time and Dose Dependent Cytotoxicity

Hugh J. Byrne
Technological University Dublin, hugh.byrne@tudublin.ie

Marcus A. Maher
Technological University Dublin, Marcus.Maher@mytudublin.ie

Follow this and additional works at: https://arrow.tudublin.ie/nanolart

 Part of the Pharmacology, Toxicology and Environmental Health Commons

Recommended Citation

Byrne, H.J. & Maher, M. (2019). Numerically modelling time and dose dependent cytotoxicity. *Computational Toxicology*, 12, 100090. doi:0.1016/j.comtox.2019.100090

This Article is brought to you for free and open access by the NanoLab at ARROW@TU Dublin. It has been accepted for inclusion in Articles by an authorized administrator of ARROW@TU Dublin. For more information, please contact yvonne.desmond@tudublin.ie, arrow.admin@tudublin.ie, brian.widdis@tudublin.ie.

This work is licensed under a Creative Commons Attribution-Noncommercial-Share Alike 3.0 License

Numerically modelling time and dose dependent cytotoxicity

Hugh J. Byrne* and Marcus A. Maher

FOCAS Research Institute,

Technological University Dublin,

Kevin Street,

Dublin 8,

Ireland

*Corresponding Author: hugh.byrne@dit.ie

Abstract

Dose-response curves are fundamental tools of *in vitro* toxicology, extensively employed in toxicant or drug screening. They are expressed by a variety of end-points and assays, measured at different time-points in a choice of cell-lines, but are typically quantified only using the mean concentration for 50% response (e.g. drug efficacy or pathway inhibition) as an indicator of overall effect. However, the response is the result of a complex and dynamic cascade of events which occur between the initial exposure and the measured end-point, and the characteristic rates of the contributing stages govern the dose response and ultimately the measured characteristic concentration. A better understanding of the effects and interdependencies of these can help in interpreting the response curves. The system can be

modelled according to a phenomenological rate equation approach, in which each stage of the process is characterised by a rate constant, and causal relationships between different processes are incorporated. The current study utilises such an approach to simulate some common response cascades of cell populations to exogenous agents and explores the dependences of the dose dependent response on, for example, number of steps in a cascade, time-point, and scenarios such as additive, synergistic and antagonistic response of multiple exogenous agents.

Keywords: *In vitro* toxicology, Numerical Modelling, Rate Equation Approach, Systems Biology.

Introduction: What's in a dose response curve?

Quantification of the efficacy of a drug, the safety of a material or the severity of a toxicant is a key component of a range of fundamental research and product development activities. Given the drive for a reduction in the use of animal models for drug testing and evaluating toxicity, due to regulatory developments in both the EU[1] and US[2], the availability and continued development of *in vitro* models for this purpose is critical. *In vitro* testing of pharmaceuticals, pesticides, or toxicants is commonly performed according to a dose response curve, the response of a cytological assay as a measure of a biological endpoint in a cell population exposed to systematically varied doses of the exogenous agent of interest. Dose response endpoints can include viability assays, but also assays from all stages of cellular toxicity pathways[3], such as xenobiotic metabolism, receptor mediated effects, and adaptive stress responses. The dose response curve is commonly fitted with an analytical function which describes the sigmoidal response behaviour, based, for example (amongst numerous others), on the Hill equation[4], and the response can be quantified in terms of the concentration required to induce a 50% response in the assay of choice, often considered in terms of inhibition (IC_{50}) or efficacy (EC_{50}). (For simplicity, the term IC_{50} is used throughout this manuscript). The protocols are well established in scientific research and, increasingly, high content screening platforms based on such assays are employed in government screening programmes and pharmaceutical drug development[5,6]. By integrating *in vitro* cytotoxicity and quantitative structure activity relationship (QSAR) approaches, predictive models can be developed to further guide screening and drug discovery strategies[7,8].

Although dose response curves are regularly and routinely employed, they are rarely analysed further than the determination of an IC_{50}, and subtle variations in the nature of the responses

are not well understood. The dose dependent response is a convolution of uptake of the exogenous agent, intracellular transport and interactions, resulting in a complex cascade of cellular processes, including activation of cellular defence mechanisms, leading to an end point response as measured by one or more cytotoxicity assays. The original Hill model is based on an analytical approach to describing ligand receptor binding in terms of equilibrium rate constants[9], in which the Hill coefficient or slope, describing the degree of curvature of the sigmoidal response, provides a quantification of the degree of interaction between ligand binding sites. Black and Leff[10] introduced the *operational model of agonism* to help further understand the action of agonists and partial agonists, and how they influence the dose-response curves. The response curves can also be represented as a Taylor series expansion, for a more generic approach to modelling responses of biological systems[11].

The response of a cellular system to exposure to an exogenous agent is a dynamic process, however, and a dose-response curve at a fixed time point provides only a snapshot of the dose dependent response which evolves systematically as a function of time. Cellular physiology is a complex, dynamic system of highly synergistic processes, and a fundamental and integrated understanding of whole cell function is required for understanding the origin and progression of disease, optimisation of therapies, and understanding of resistance and sensitivity of cells to therapy, as well as the development of ever improved imaging technologies. Notably, such complex multivariant systems are not unfamiliar to the realms of the physical and chemical sciences, but are rather considered in an evolutionary sense. Systems Biology approaches to representing and understanding the mammalian cell metabolism are becoming increasingly sophisticated[12],[13] and include such physicochemical models to represent the system properties, behaviour, and observable characteristics. In a

systems biology approach, the structure and dynamics of the different cellular functions are examined, instead of the characteristics of the individual cellular components. Each of the analytical or numerically soluble equations in the model can be associated with a specific process in the system, and hence each of the parameters, rates and initial conditions, can be assigned a physical/biochemical interpretation in the overall model of the system.

In a cell population, the system can be modelled in a phenomenological rate equation approach, similar to that used by Einstein to describe population photodynamics, and predict the phenomenon of laser action[14]. The approach has been used to model and understand the complex cascade of photoinduced effects in nonlinear optics of materials and photochemistry[15]. The dose dependence at a certain time point reflects the temporal evolution of the system to the initial perturbation to the system and can be used to model transient (pulse chase) or steady state exposures. The use of such rate equation models for the simulation or fitting of complex systems has become increasingly prevalent in pharmacokinetics/pharmacodynamics[16,17]. In terms of nanobio interactions, Salvati *et al.* employed a rate equation approach to model the uptake of polystyrene nanoparticles in cells as measured by the fluorescent response of the cell populations, although no modelling of the cellular responses was undertaken[18]. Dell'Orco *et al*. used a similar approach, described in terms of Systems Biology, to model the delivery success rate of engineered nanoparticles and its dependence on the presence and structure of the protein corona[19]. Maher *et al.* utilised such an approach to describe the generation dependent uptake of, and subsequent oxidative stress and immune-responses to, poly amido amine (PAMAM) dendrimers *in vitro*, accounting for the differing responses of different cytotoxicity assays and cell lines[20], and

Dadalt-Souto *et al.* similarly simulated the *in vitro* response to drug loaded chitosan nanoparticles[21].

The representation of the cellular responses in terms of a causally related sequence of events leading to cell death in terms of uptake, interaction and response rate constants provides a more intuitive representation of the state of the system and the dependences of the process on the physico-chemical nature of the exogenous agent, the cell type and the cytotoxic assay/end point. It therefore lends itself more naturally to platforms of predictive toxicology, such as QSARs[22] and the Adverse Outcome Pathway (AOP) formalism[23]. This paper will explore the temporal and dose dependent responses of cellular systems to the exposure to exogenous agents using a phenomenological rate equation approach to illustrate the effects of different uptake and response processes, as well as experimental protocols, on the measured response, and therefore the wealth of information which underpins cytotoxicity response curves. The simulations apply generically to cell populations, and no experimental data is explicitly used. However, reference is made to specific experimental studies throughout, and the rates and timescales are guided by previous experimental studies of the interactions of nanoparticles and drugs with cells in vitro, from the authors[20,24–26].

Methodology:

An exogenous agent, in molecular or particulate form, is uptaken by a cell by, for example, pino- or endo- cytosis, whereupon it initiates a biochemical response in the cell. In the case of intercalating chemotherapeutic agents such as doxorubicin (DOX), this occurs via rapid uptake and transport to the nucleolus/nucleus of the cell (~4-12 hrs), whereupon it

intercalates with the RNA/DNA, initiating a toxic response, leading to apoptosis[27]. In the case of cationic nanoparticles, endocytosis results in ROS generation in the endosomes/lysosomes, oxidative stress, loss of mitochondrial membrane potential, and initiation of inflammatory responses[28].

The latter case has previously been numerically modelled for the case or PAMAM dendrimers, and is illustrated schematically in Figure 1[20,29]. In particular, the schematic representation depicts the uptake of a particle by a cell (system), progression to ROS generation (quenched by anti-oxidants), then onto mitochondrial damage, inflammatory cascade and finally apoptosis (if the cellular recovery rates are insufficient). The system could equally be adapted to represent the uptake of a toxicant or chemotherapeutic agent, in the latter case, for example, its intercalation in the nucleus, resulting in RNA/DNA damage and subsequent apoptosis. The model can be adapted to incorporate any number of intermediate steps to embellish the description of the mode of action and/or cellular response pathways, including cell recovery mechanisms.

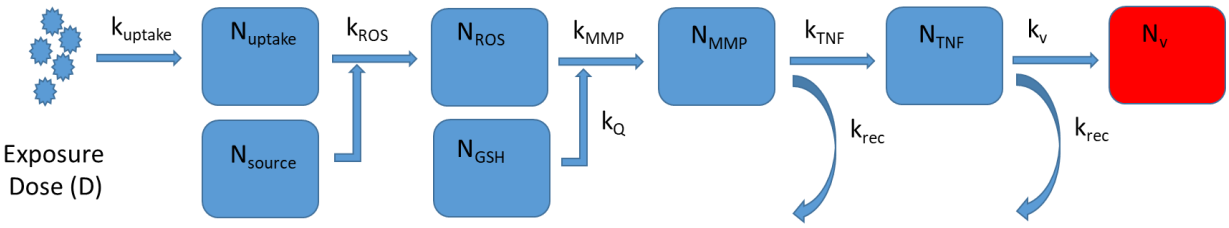

Figure 1: Schematic representation of systematic sequence of events upon uptake of exogenous agent (nanoparticle). The rates (k) and numbers (N) of each step describe, respectively, cellular uptake, ROS generation, antioxidant (GSH) quenching, mitochondrial membrane potential (MMP) decay, tumour necrosis factor (TNF), and loss of viability (v). The term "source" is implicated in the intracellular generation of ROS, while "rec" indicates routes of recovery.

The complex system illustrated schematically in Figure 1 can be better described using a series of rate equations, as described in detail by Maher *et al.*[20]. The series of equations and their impact on the modelling process and dose response curve are introduced sequentially in the Results section. Numerical results for all equations were obtained by integration using the iterative Euler approach[30] and Matlab (v.2018b) was used to generate the model and data. Sigmaplot v10 was employed to analyse the dose response curves using the Pharmacological Curve fitting procedure of a four parameter Hill equation:

$$f(x) = min + \left(\frac{max - \min}{1 + \left({}^{x}/_{IC_{50}}\right)^{n}}\right) \qquad \text{Equation (1)}$$

in which the Hill slope is represented by *n*.

Results

The process of nanoparticle endocytosis by cells *in vitro*, taking into account the cell replication rate (k_{doub}), has previously been described by Salvati *et al.*[18] and subsequently by Maher et al. [31] and is here represent by Equation 2, in which a generalised case of nanoparticle or molecule uptake is considered. As the dose (*D*) is expressed as the molar dose, for ease of comparison with the experimental data, N_{uptake} is an expression of the molar quantity (number per unit volume) of uptaken nanoparticle or molecule. In subsequent equations, the term "*N*" is used to denote the equivalent quantity denoted by the subscript text that follows.

$$\frac{dN_{uptake}}{dt} = \left(D - N_{uptake}\right)\left((1 + k_{doub}).N_{cell}.k_{uptake}\right) \qquad \text{Equation (2)}$$

where k_{uptake} is the rate of endocytosis (in units of inverse time), k_{doub} accounts for cellular replication during the exposure period and D is the molar dose. Assuming a cell duplication half life of 24hrs, k_{doub} has a value of $(0.69/24)hr^{-1}$.

In the absence of cell replication or depletion of the applied dose, as represented by the term (D-N_{uptake}), the uptake of the exogenous agent by the cell population N_{cell} is a linear function of time, as shown in Figure 2. Depletion of the applied dose by the uptake process introduces a nonlinearity in the uptake process, however, and the impact of this depletion is dependent on the rate of uptake, as might be expected. The process also depends on the number of cells, and so the endocytosis rate is best considered as a rate per unit time, per cell.

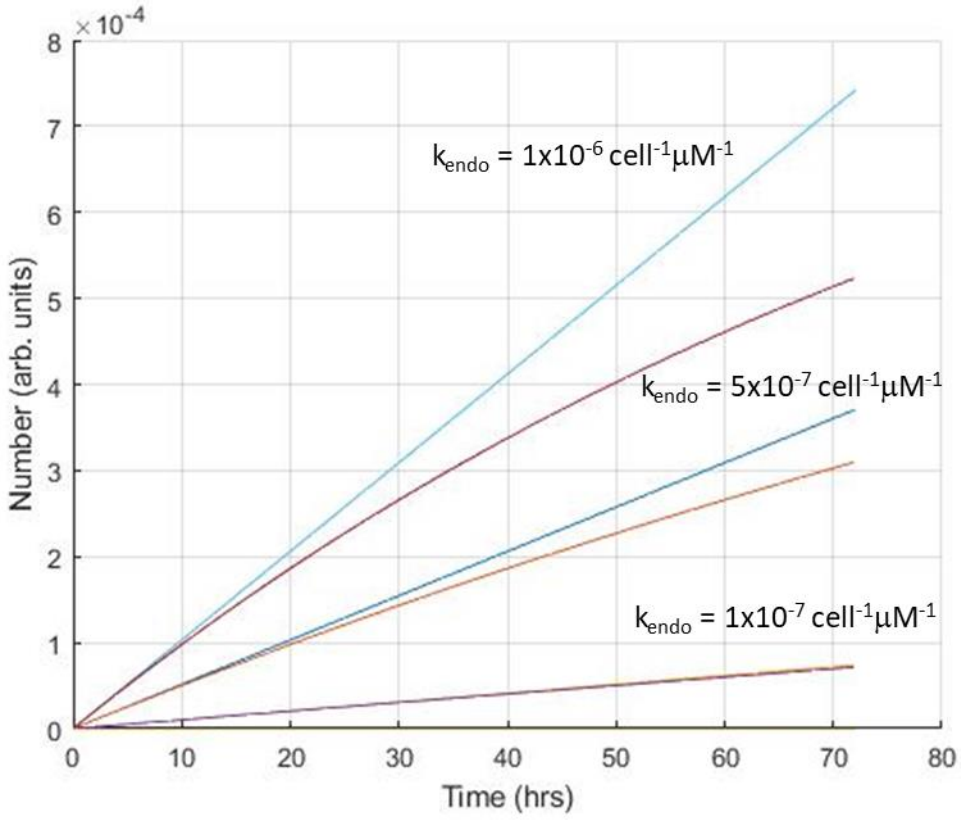

Figure 2: Internalised dose (N_{uptake}) as a function of time, with (linear) and without (curved) source depletion, for different uptake rates, k_{endo}.

In a very simplistic model, the uptake of the exogenous agent can be considered at this stage to impact on the cell viability, N_v, initially set equal to a value of 1 to represent 100% cellular viability, such that

$$\frac{dN_V}{dt} = -k_V . N_{uptake} . N_V \qquad \text{Equation (3)}$$

Using Equation 3, the dose dependent loss of viability can be represented as a dose response curve, as shown in Figure 3. The response was calculated for parameters of $N_{cell} = 10^5$, $k_{uptake} = 10^{-7}$ cell^{-1}hr^{-1} and $k_v = 0.1$ μM^{-1}hr^{-1}, at a timepoint of 24 hrs. The dose-response curve matches well that generated by a four parameter Hill equation (Equation (1)), with the exception of the curvature at the low and high dose ends. It should be noted, however, that at this stage the model does not include many confounding factors of the intracellular processes, to be introduced in later aspects of the study, and also that the Hill model is not the only model appropriate to dose response curves[5]. Critically, it is important to bear in mind that the model is continuous in both dose and cell number, rather than discrete in terms of individual molecules or cells, and in particular does not account for multiple dosage of an individual cell.

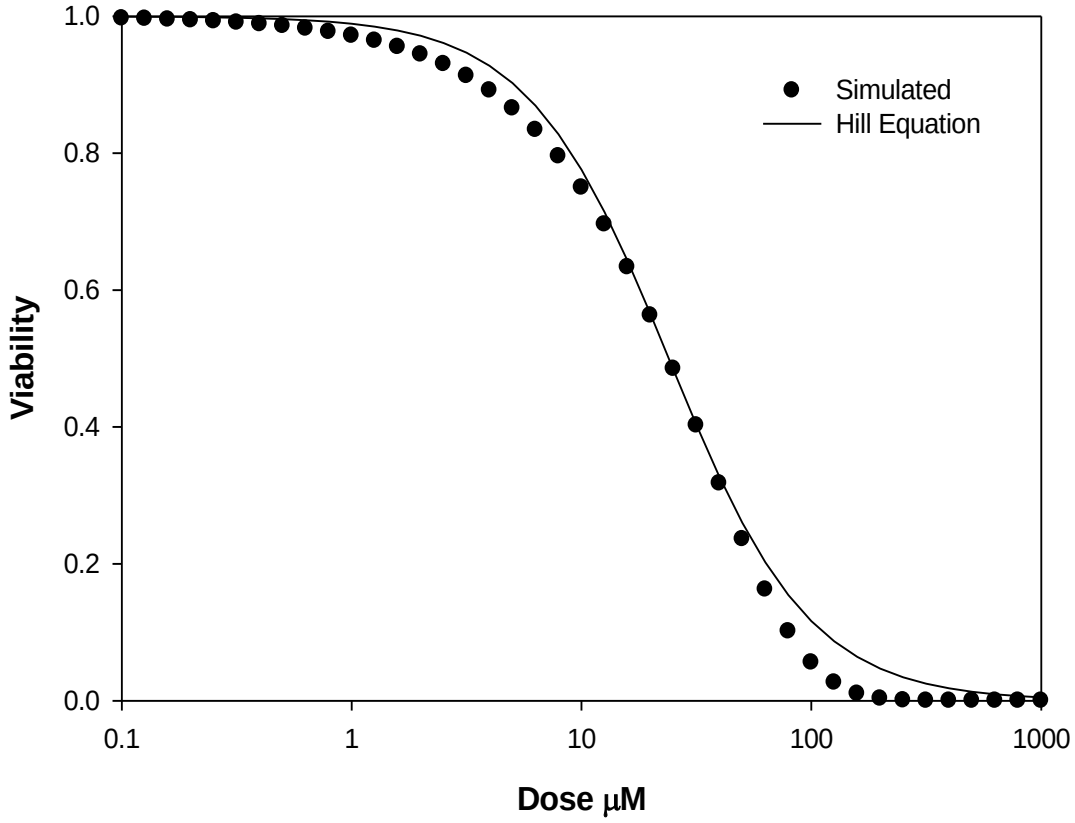

Figure 3: Dose Response curve calculated according to Equation (3) (dots) for a 24hr timepoint, compared to a four parameter Hill curve (solid line).

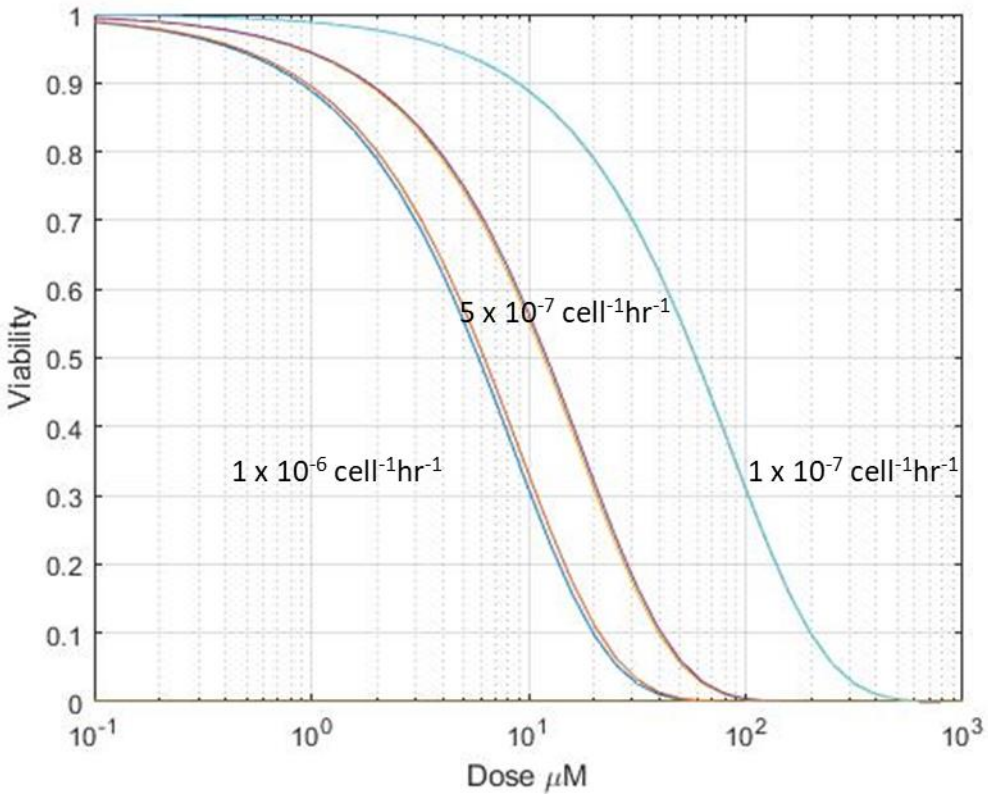

Figure 4: 24hr dose response curve and its dependence on uptake rate, with and without source depletion. Source depletion results in an only slightly higher IC_{50} value, perceptible for the 1 x 10^{-6} $cell^{-1}hr^{-1}$ curve.

In this simple model, the dose response is primary effected by the uptake rate, as shown in Figure 4. The impact of dose depletion is relatively small, although this does depend on the uptake rate, but also the timepoint at which the reduction in viability is measured. The dose response curve is also critically dependent on the fixed timepoint at which the loss in viability is measured, as shown in Figure 5. Notably, a higher degree of toxicity is registered with increasing exposure time, as might be expected, and this is best represented by the inverse IC_{50}[32], which is seen to be a complex function of exposure time, as shown in the plot of Figure 6. Furthermore, although the general shape of the curves in Figure 5 appears to be independent of exposure time, the Hill slope of a four parameter fit is seen to be exposure

time dependent, as shown in Figure 7. Such a complex relationship of inverse IC_{50} with exposure time has been observed for the action of chemotherapeutic agents, and is understandable by considering that the endpoint or exposure time is shorter that any of the times associated with the critical rates of the cellular processes[33]. In the case of Figure 6, it can be considered that the trend of toxicity, as represented by the inverse IC_{50}, is lower than expected for times of <24 hrs, given that the rate of loss of viability is 0.1 hr^{-1}, with an associated timescale of 10 hrs.

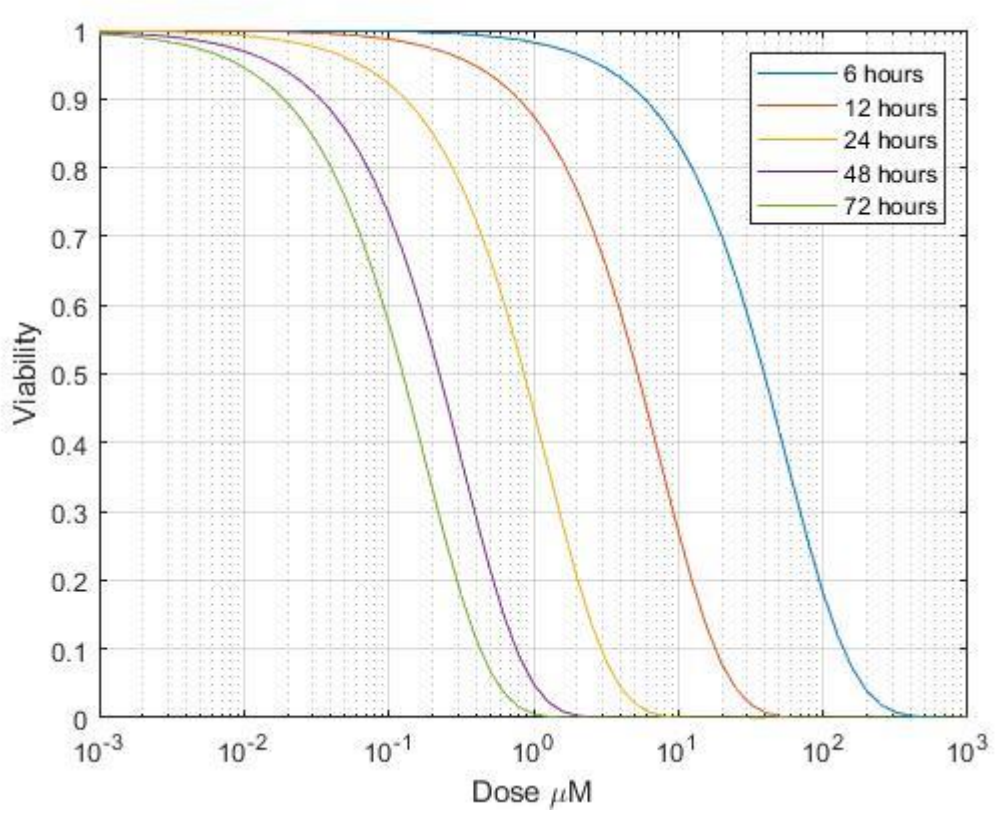

Figure 5: Dependence of Dose Response on exposure time (no depletion)

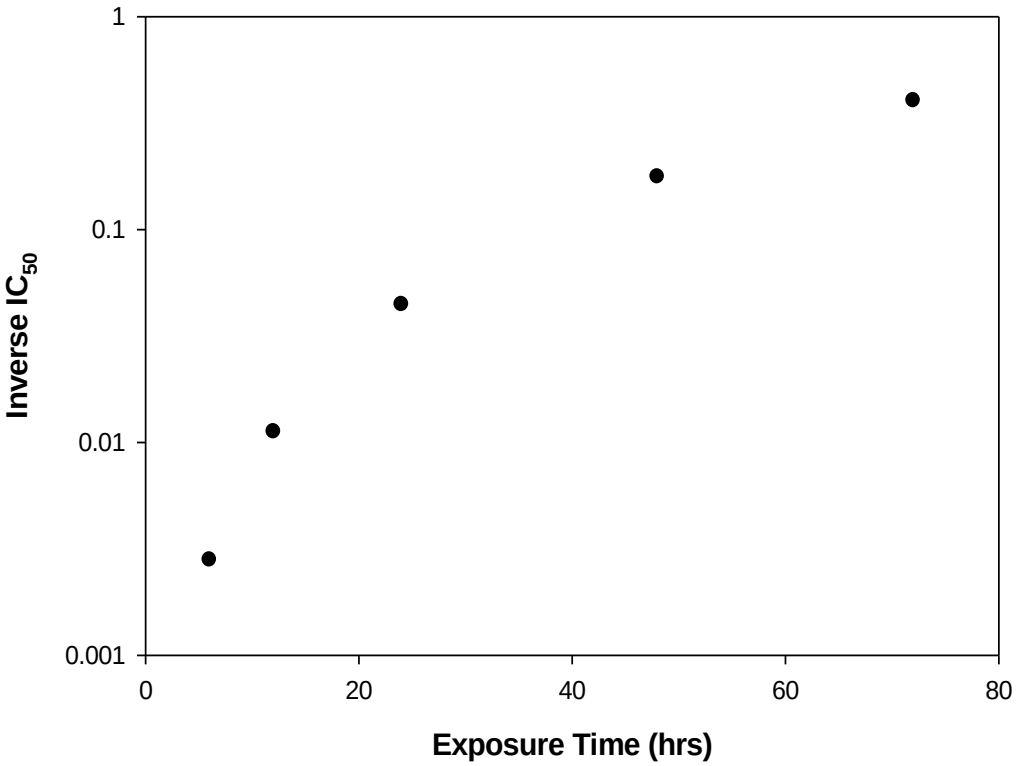

Figure 6: Dependence of (inverse) IC_{50} on exposure time. Individual dual data points are derived from the simulations of Figure 5.

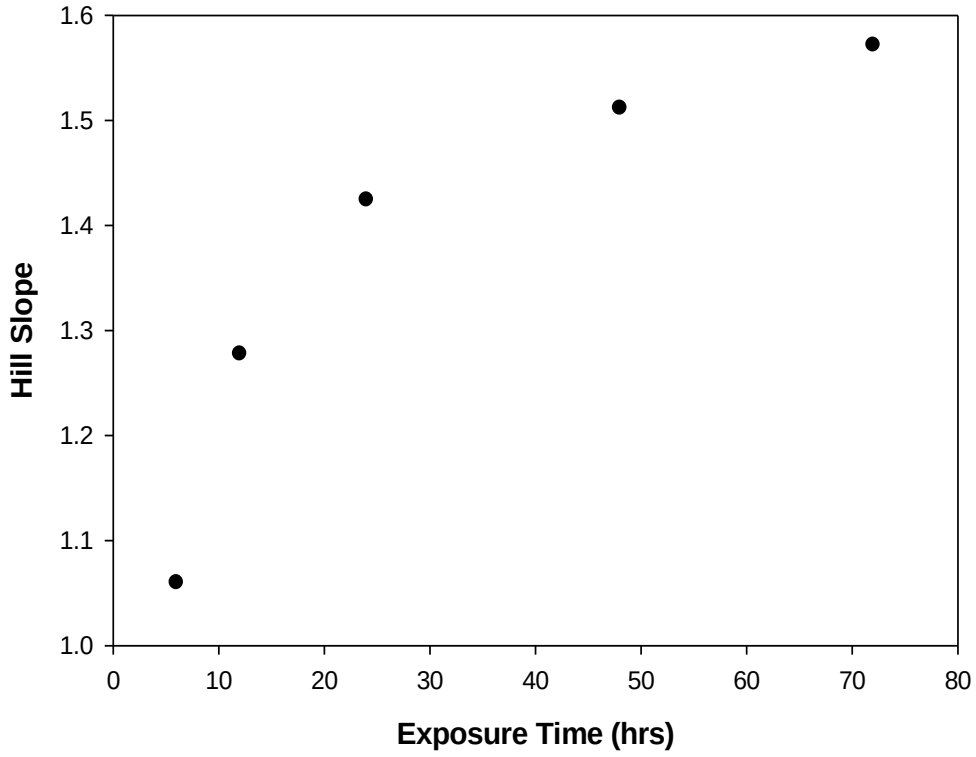

Figure 7: Dependence of Hill Slope on exposure time. Individual dual data points are derived from the simulations of Figure 5.

Although it can simulate many features of the common dose response curve, the model of Equation 3, based on a direct response to uptake of an exogenous agent, is greatly simplified, and does not include many aspects of the cellular response processes. In the case of cationic nanoparticles, endocytosis results in the generation of ROS and the resultant oxidative stress is counteracted by the intrinsic intracellular anti-oxidants, exemplified previously by the intracellular levels of glutathione (GSH), and the interaction quenches both the levels of ROS and GSH[29]. In the previous study which modelled the dose and time dependent toxicity of PAMAM dendrimers, it was determined that, in order to accurately model the system, a further, exhaustible ROS "Source" term, N_{Source}, should be introduced[20]. In a similar way to

binding receptors for drugs, this term limits the extent of the interaction of the toxicant in the cell. Thus:

$$\frac{dN_{Source}}{dt} = -N_{endo}.N_{Source}.k_{ROS} \qquad \text{Equation (4)}$$

where k_{ROS} is the interaction rate for the nanoparticles and source. The generation of ROS is then described by:

$$\frac{dN_{ROS}}{dt} = N_{endo}.N_{Source}.k_{ROS} - N_{GSH}.N_{ROS}.k_q \qquad \text{Equation (5)}$$

$$\frac{dN_{GSH}}{dt} = k_{GSH} - N_{GSH}.N_{ROS}.k_q \qquad \text{Equation (6)}$$

The first term in Equation (5) is a dose (*D*) dependent term describing continuous ROS generation at a rate k_{ROS} ($N_{ROS}(0) = 0$). The second term describes the quenching of the ROS at a rate k_q, and depends on both; ROS levels, N_{ROS}, and antioxidant levels, N_{GSH} ($N_{GSH}(0) = 0$). In the study by *Mukerjee et al.*, the antioxidant levels were represented by the experimentally measured values of Glutathione (GSH).[38] In Equation (6), the experimentally observed linear increase of the control levels of GSH, at a rate of k_{GSH}, is described by the first-term, and the second-term, which is the same as in Equation (5), describes the quenching of the GSH levels. Values of k_{GSH} and k_q are derived from the experimental data and simulations of Mukherjee *et al*.[29]

Figure 8 shows the effect on the time dependence of the generation of ROS as a function of N_{source}, at a fixed value of k_q=0.005hr^{-1}. Note, that the maximum value has been normalised to 1 for each value of N_{source}, for visualisation purposes. The maximum level of ROS increases significantly as the value of N_{source} increases, but equally, so too does the impact of the

quenching process. For a fixed value of N_{source}=10, Figure 9 shows the effect of varying rates of quenching interaction rate, k_q on the normalised profile of ROS generation. In this case, the absolute magnitude of ROS is decreased with increasing rate, as might be expected, and the maximum of the oxidative stress profile shifts to shorter times. The increased rate of antioxidant quenching of ROS is to reduce the toxicity of the exogenous agent, as can be seen by the shifting of the dose response profile to higher doses, as seen in Figure 10. For fixed N_{source} (=10) and k_q (=0.005 hr^{-1}) the effect of increased dose on the time evolution profile of the ROS is to increase the magnitude of the maximum, continuously shifting to earlier times, as shown in Figure 11. A similar behaviour was observed for the generation and dose dependent oxidative stress profiles of PAMAM dendrimers[29].

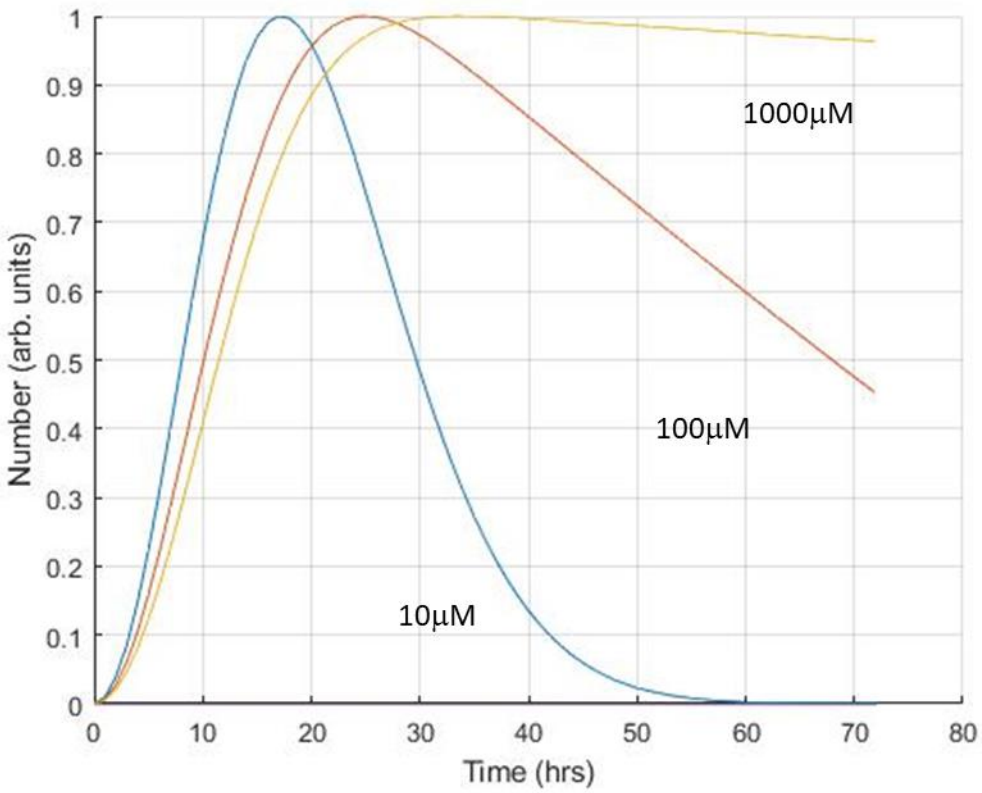

Figure 8: Dependence of (normalised) time evolution of N_{ROS} on N_{source}: (Dose =10^3 μM)

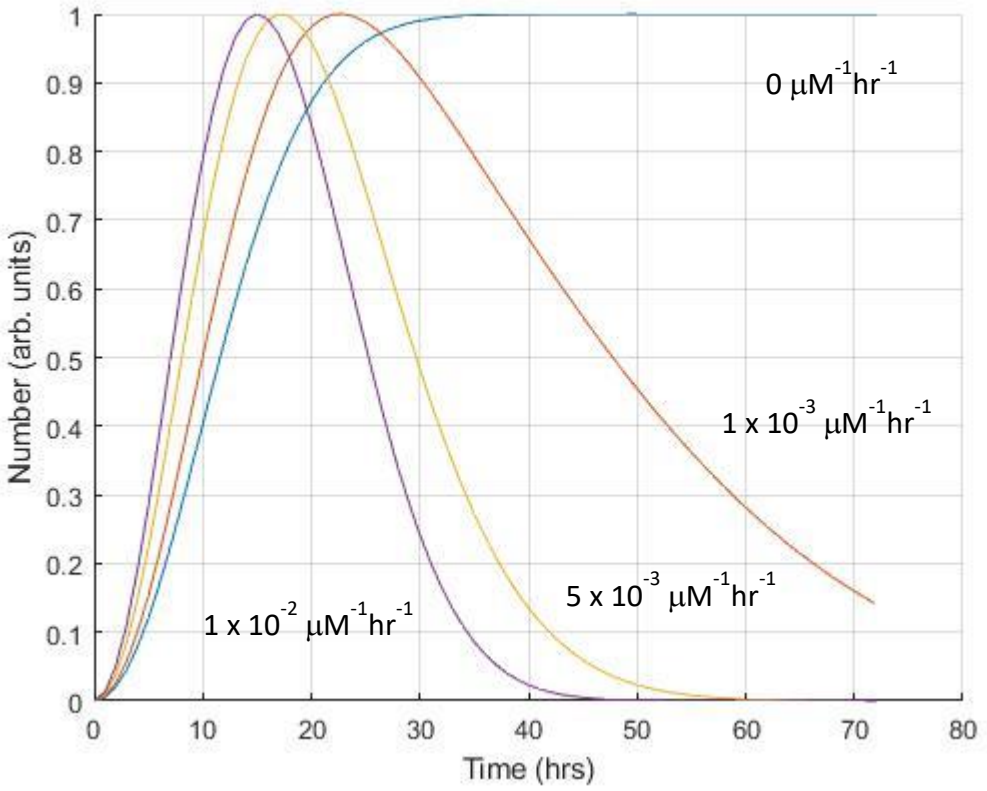

Figure 9: Dependence of (normalised) time evolution of N_{ROS} on k_q: (Dose =10^3 μM)

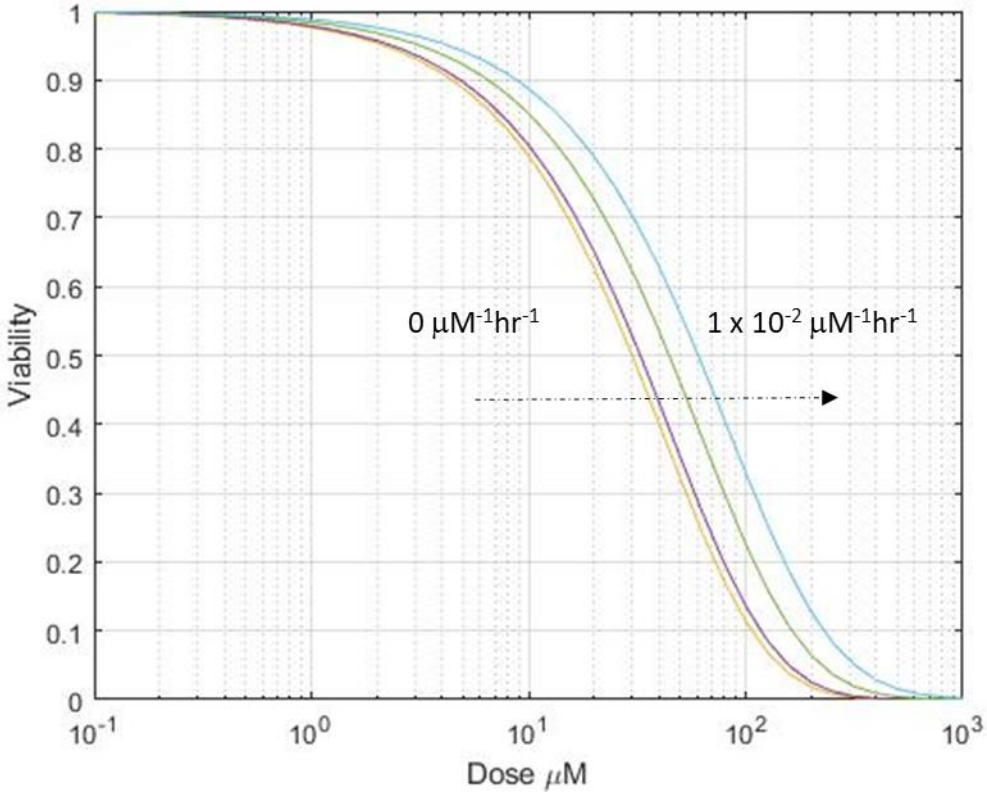

Figure 10: Dependence of Dose Response curve (at 72 hrs) on k_q

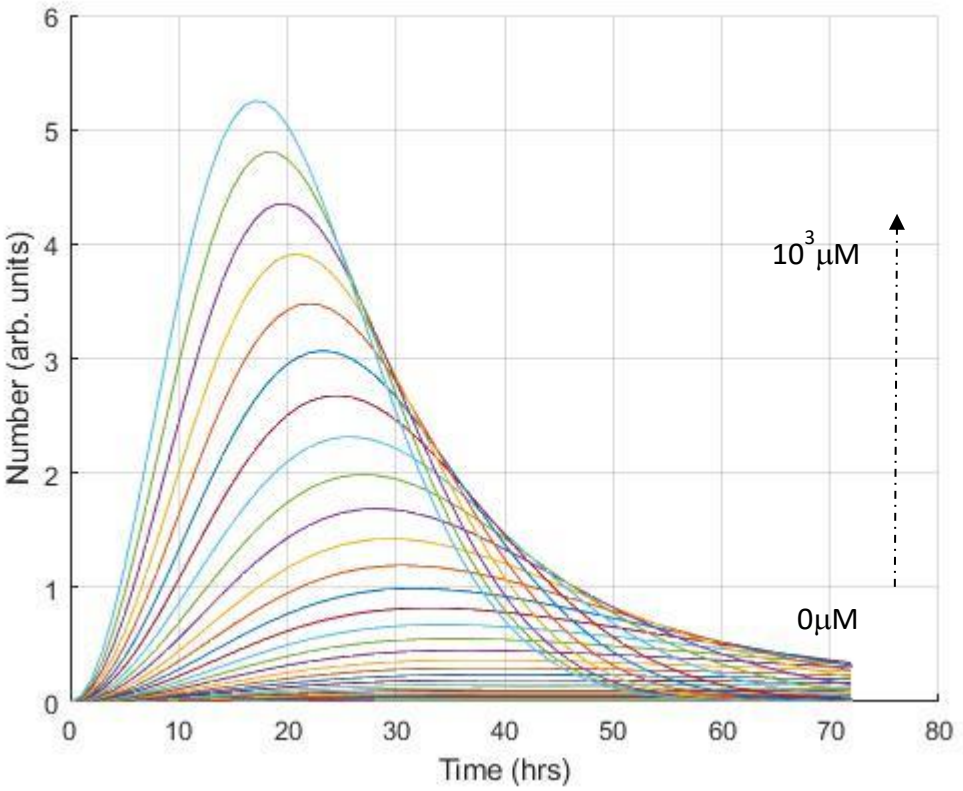

Figure 11: Dose dependence of time evolution of N_{ROS}.

The subsequent, experimentally observed, cascade of cellular responses can be similarly simulated. In the case of the experimental studies of PAMAM dendrimer nanoparticles, the cascade elements examined were: caspase activation, mitochondrial membrane potential decay (MMPD), generation of tumour necrosis factor alpha (TNF-α) and interleukin-8 (IL-8) for HaCaT cells[25], or interleukin-6 (IL-6) for mouse macrophages[32]. In the model of Mukherjee *et al.,*[29] the early stage caspase activation and MMPD are both a result of increased levels of ROS, although through independent pathways. Thus:

$$\frac{dN_{Casp}}{dt} = k_{Casp}.N_{ROS} - k_{Casp2}.N_{Casp} \qquad \text{Equation (7)}$$

$$\frac{dN_{MMP}}{dt} = k_{MMP}.N_{ROS} - k_{TNF}.N_{MMP}$$ Equation (8)

$$\frac{dN_{TNF}}{dt} = k_{TNF}.N_{MMP} - k_{IL-8}.N_{TNF}$$ Equation (9)

$$\frac{dN_{IL-8}}{dt} = k_{IL-8}.N_{TNF}$$ Equation (10)

Again, in Equations 7 to 10; *N* describes the respective populations at time *t*, and *k* the respective rates and the initial conditions for all cases are such that *N(0) = 0*. Overall, these equations show a possible cascade of events as a result of oxidative stress involving; parallel rather than sequential processes of caspase activation and loss of MMP, the latter leading to activation of TNF-α and IL-8, as described for (HaCaT) human skin cells, exposed to PAMAM dendrimers by Mukherjee *et al*.[29].

Figure 12 shows the (normalised) evolution of the ROS, MMP and TNF-α as a function of time. The values for the respective parameters employed are listed in Table 1.

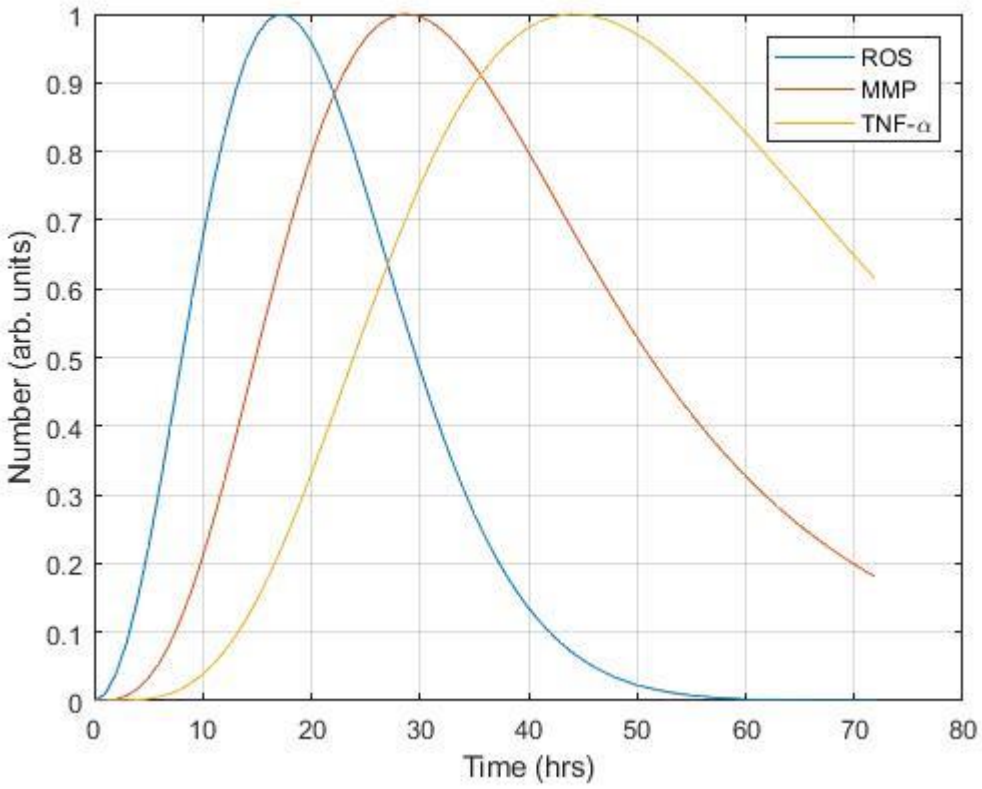

Figure 12: Time evolution of (normalised) the cellular ROS, MMP and TNF-α (Dose = 10^3μM)

Table 1: List of Model Parameters, unless otherwise stated

Morel Parameter	**Value**
N_{Cell}	10,000
k_{endo}	1 x 10^{-5} $cell^{-1}$ hr^{-1}
k_{doub}	0.03 hr^{-1}
k_{ROS}	1 x 10^{-3} μM^{-1} hr^{-1}
k_q	5 x 10^{-3} μM^{-1} hr^{-1}
k_{GSH}	1 hr^{-1}
k_{v1}	0.5 μM^{-1} hr^{-1}

k_{MMP}	0.05 hr^{-1}
k_{v2}	0.05 μM^{-1} hr^{-1}
k_{TNF}	0.05 hr^{-1}
k_{v3}	0.025 μM^{-1} hr^{-1}
k_{IL8}	0.05 hr^{-1}
k_{Casp}	0.05 hr^{-1}
k_{Casp2}	0.05 hr^{-1}
k_{v4}	0.01 μM^{-1} hr^{-1}

Loss of cell viability can be monitored using a number of assays.[16,17] As an example, the 3-(4,5-dimethylthiazol-2-yl)-2,5-diphenyltetrazolium bromide (MTT) assay measures the mitochondrial activity and is thus experimentally most associated with changes in the mitochondrial membrane potential, loss of which can, at certain levels, lead to apoptosis. The following equation can be used to calculate the change in the population of viable cells, N_V as a result of any of the calculated cellular responses N_x, representing either N_{ROS}, N_{Casp}, N_{MMP}, N_{TNF}.

$$\frac{dN_V}{dt} = -k_V . {N_x}^b . N_V \qquad \text{Equation (11)}$$

Equation 11 describes the process of cell death, dependent on the change in the cellular response, and the number of viable cells. N_V is initially set equal to a value of 1 to represent 100% cellular viability. The significance of the stochastic term *b* will be explored at a later stage.

Figure 13 illustrates the dose response curves for three assays, measuring the cellular oxidative stress (N_{ROS}), loss of mitochondrial membrane potential (N_{MMP}) and inflammatory response (TNF-α) at a 24hr time point. It is clear that three different assays, at the same time point, can portray what appears to be a very different toxic response, precisely because they measure processes which occur at different rates in the cell. Notably, as shown by the dashed lines, the fit of a four parameter Hill equation to the simulated response improves as the cascade progresses. Values of Hill slope, and standard errors, derived from the fit are respectively, ROS: 1.52 ± 0.04, MMP: 1.107 ± 0.004 and TNF: 0.879 ± 0.009. The fact that the modelled response improves with complexity is important when considering not just the full dose range, but also the low dose responses, as has been advocated for in vitro bioassays with environmental samples[34].

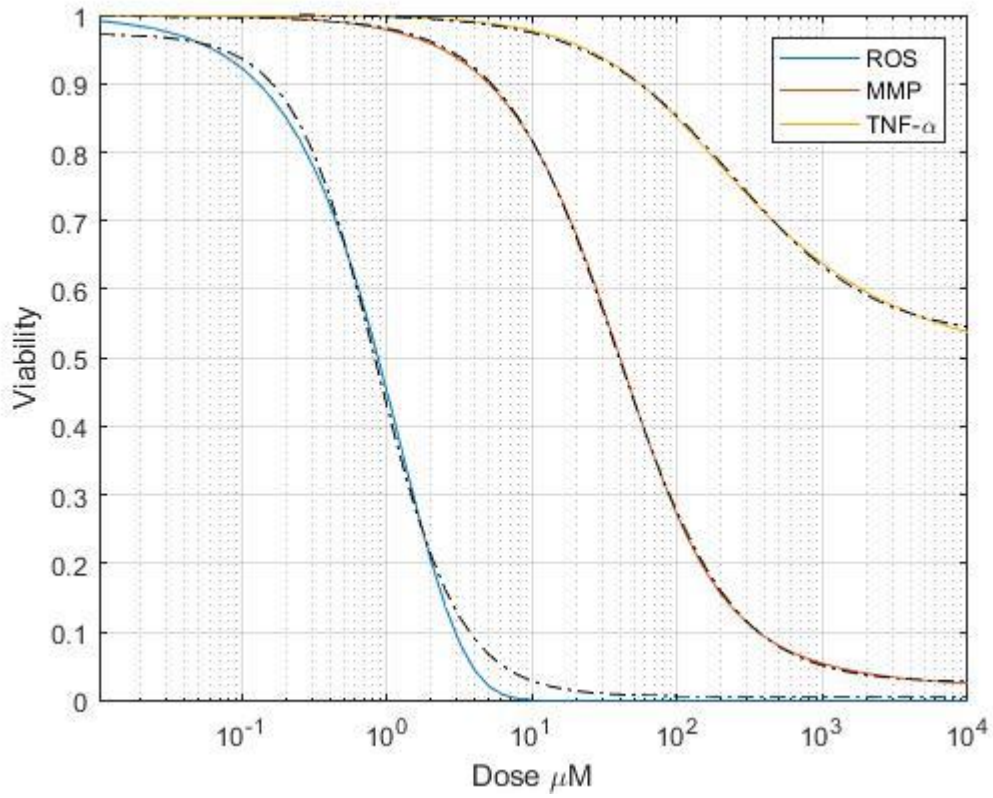

Figure 13: Dose response for three assays responsive to the cellular responses of oxidative stress (ROS), loss of mitochondrial membrane potential (MMP) and inflammatory response (TNF-α), measured at a 24hrs timepoint. The dashed lines show fits of a four parameter Hill equation to the simulated responses.

Similarly, when measured at different timepoints, any one of these assays can show very different responses, as shown in Figure 14, for the case of the TNF-α response. Again, the dashed lines show fits of a four parameter Hill equation to the simulated responses. The Hill slope of the fit to the simulated response is relatively insensitive to exposure time, varying from 0.798 ± 0.009 for 6 hrs to 0.969 ± 0.007 for 72 hrs.

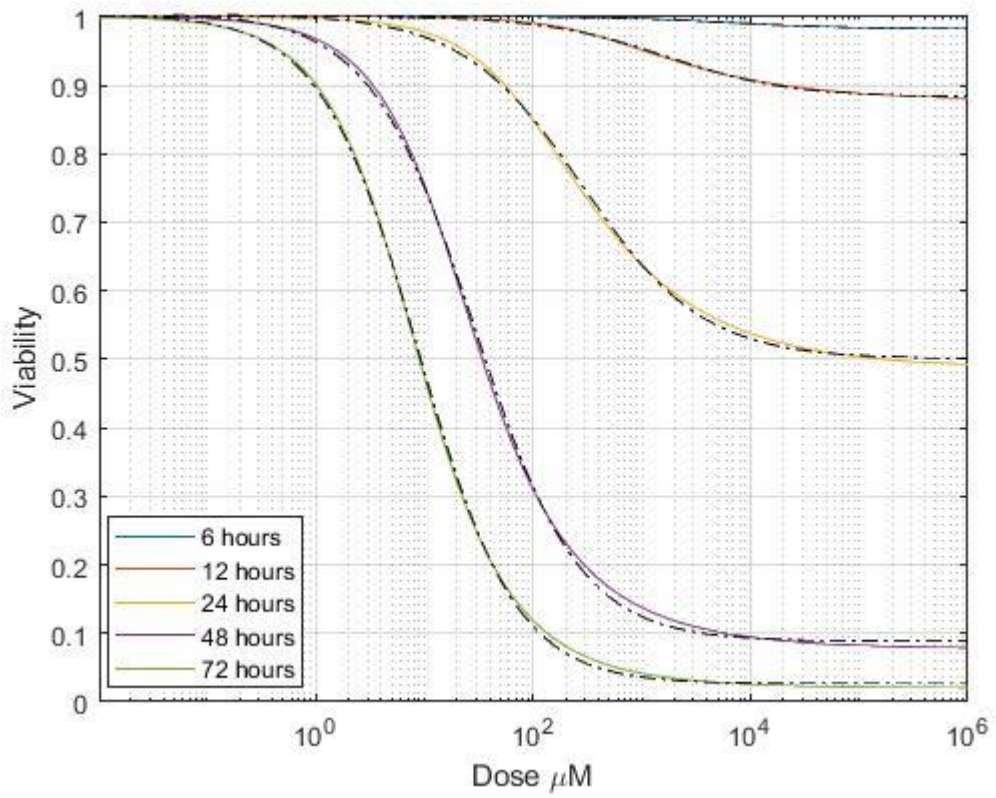

Figure 14: Dose response for the cellular inflammatory response (TNF-α), measured at different timepoints. The dashed lines show fits of a four parameter Hill equation to the simulated responses.

As indicated in Figure 1, any of the cellular response pathways can have branches for recovery, without leading to loss of viability, or other assay response. In the case of oxidative stress, antioxidant quenching provides such a mechanism. At other points in the cascade, similar quenching or recovery mechanisms can be included, as indicated in Equation 12, resulting in a reduction of N_{TNF} according to a rate k_{rec}.

$$\frac{dN_{TNF}}{dt} = k_{TNF}.N_{MMP} - k_{IL-8}.N_{TNF} - k_{rec}.N_{TNF} \qquad \text{Equation (12)}$$

The effect of such a process is to reduce the rate of response of the assay, as indicated in Figure 15, for the 72hr response with varying values of k_{rec} from 0-1 hr^{-1}.

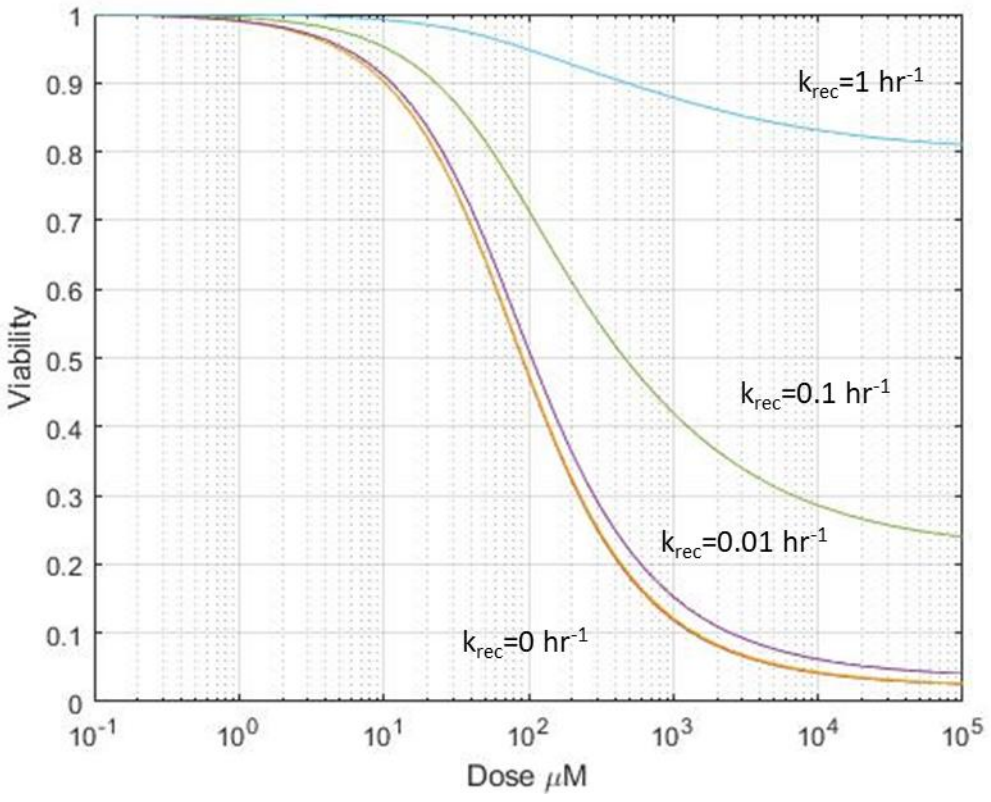

Figure 15: 72 hr Dose Response of the TNF-α assay, with varying recovery rates k_{rec}.

When measuring processes which evolve along parallel metabolic pathways, very different toxic responses are similarly registered by two independent assays, as shown in Figure 16. Caspase activation due to oxidative stress, in parallel with loss of MMP, is simulated according to Equation (7), in which k_{Casp} represents the caspase activation rate and k_{Casp2} a depletion rate. The response rate of the assay, kv_4, is set at 0.01 hr^{-1}, compared to the MMP assay response rate of 0.05 hr^{-1}. Note, where the generation and response rates are equal for both pathways, the assays exactly overlap, but a difference in response rates results in a significantly different dose response curve at this time point, although the dose responses will equilibrate at later time points. Such behaviour is common when using two different assays, such as Alamar Blue, which is used as a measure of general cell metabolic activity, and MTT, more sensitive to changes in mitochondrial activity[35].

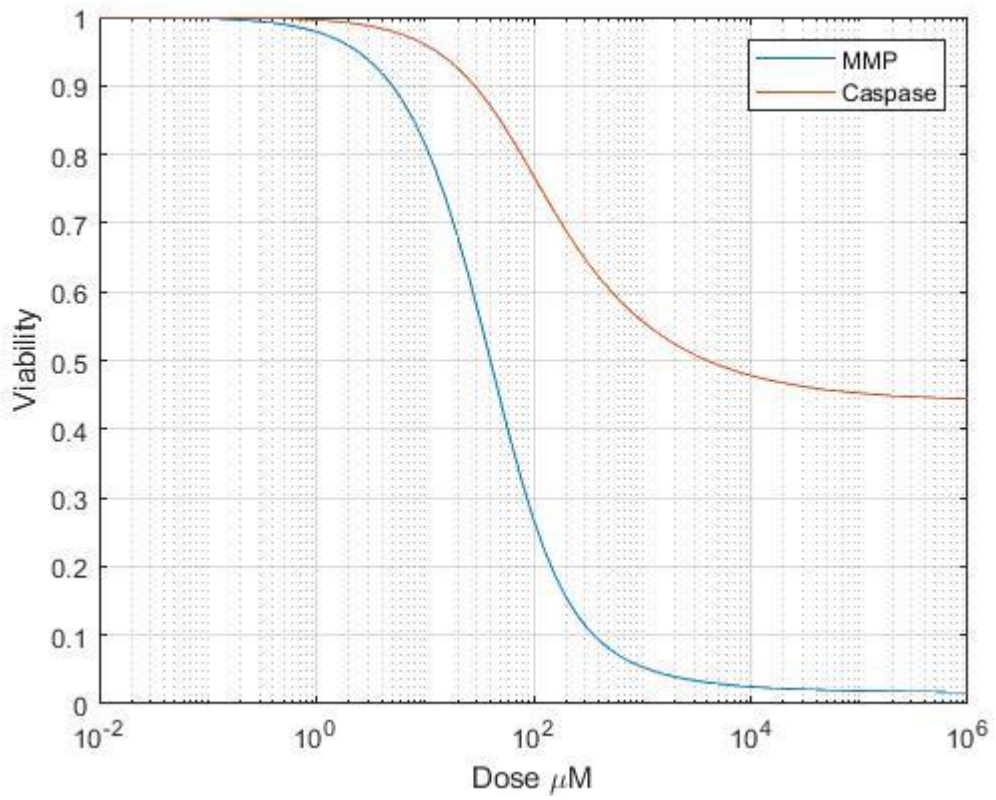

Figure 16: Dose dependence of loss of viability due to the parallel processes of Caspase activation in the cytoplasm and loss of mitochondrial membrane potential, at 24 hr exposure time.

It is noticeable that, in the dose response curves of Figures 13-16, many do not reach a value of zero. However, as shown in Figure 14, this can be the result of a short exposure time in comparison to the cellular response time, and does not represent a phenomenon of "partial agonism". In the context of agonist-receptor binding, as a model for example of the intracellular mechanism of action of drugs, a partial agonist can bind in different ways, some of which do not activate the expected the cell signalling pathway[36]. In the model presented in Equations (1-6), such a partial agonism can be represented through the interaction of the uptaken agent with the reaction source. In the case of ROS generation, an alternative reaction route can be represented, such that the binding, at rate k_b, gives rise to bound species, N_{bound}, according to Equation (12) which do not result in the generation of ROS, but deplete the available reaction source, N_{Source}, according to Equation (13):

$$\frac{dN_{bound}}{dt} = N_{uptake}.N_{Source}.k_{binding} \qquad \text{Equation (13)}$$

$$\frac{dN_{Source}}{dt} = -N_{uptake}.N_{Source}.k_{ROS} - N_{uptake}.N_{Source}.k_{binding} \qquad \text{Equation (14)}$$

In this simplistic phenomenological model, which does not explicitly consider the response of individual cells in an ensemble, the cellular response, resulting in the change in the assay, is represented by $(1\text{-}N_v)$ as calculated by Equation (11). Considering that N_{bound} do not contribute to the cellular response pathway, this should be normalised by the ratio $(N_{Source} - N_{bound})/N_{Source}$, and the resultant assay response, over the range 1-0 is represented by $(1\text{-}N_{v'})$, where $N_{v'}$ represents the normalised response. Figure 17 represents the response of an assay

monitoring the loss of viability due to ROS, with increasing amounts of N_{bound}, as a result of increasing values of k_b. The result is primarily to increase the level at which the dose response saturates from 0, to a value which is equal to (k_{ROS} x k_b)/(k_{ROS} + k_b). Also shown are examples of the effect of varying ROS generation rates, k_{ROS}, at fixed k_b. In this case, the dose response shifts to higher (k_{ROS}, = 5 x 10^{-4} μM^{-1} hr^{-1}), or lower (k_{ROS}, = 5 x 10^{-4} μM^{-1} hr^{-1}) doses, but notably, the high dose saturation level also shifts according to the ratio to (k_{ROS} x k_b)/(k_{ROS} + k_b), reflecting the competition between the two processes.

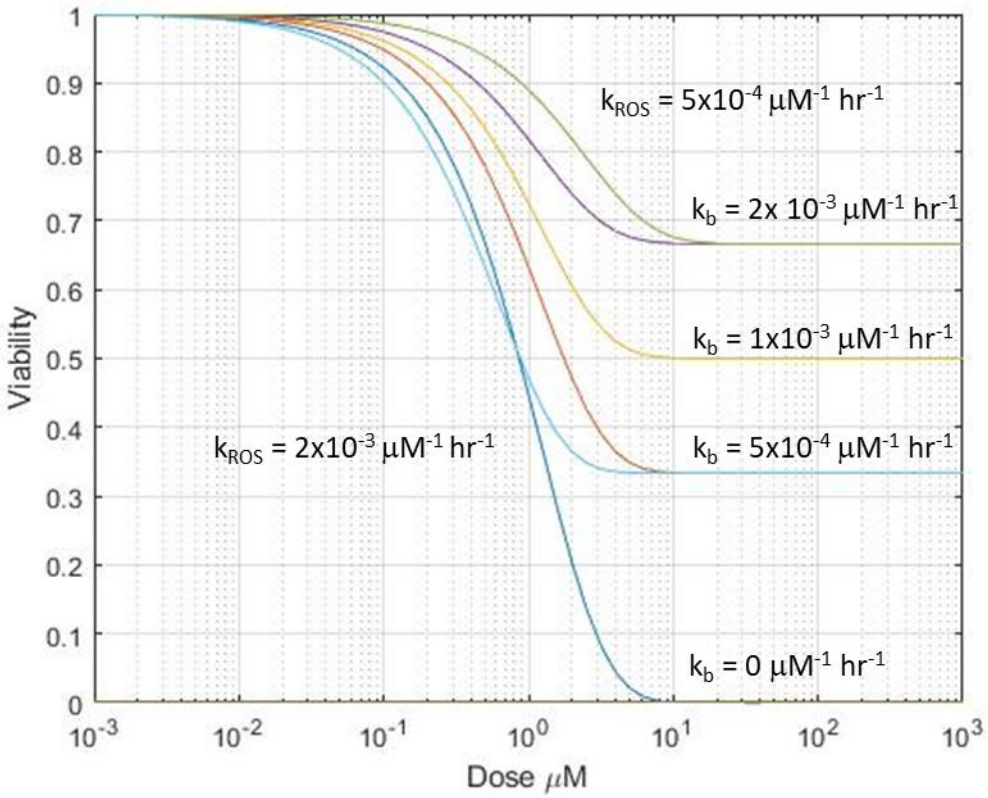

Figure 17: Dose Response curves depicting partial agonism (ROS generation, k_{ROS}= 1 x 10^{-3} μM^{-1} hr^{-1}), due to varying rates of competitive binding (k_b). Also shown are the responses at a fixed binding rate of k_b= 1 x 10^{-3} μM^{-1} hr^{-1} and varying ROS generation rate.

It should be noted that the simulations to date have presumed a 1:1 stoichiometric ratio of the reaction species. However, as represented by the parameter *b* in Equation 11, this ratio can vary depending on the nature of the reaction. A variation in the stoichiometric ratio has a significant effect on the dose response curve, as shown in Figure 18, for the case of Caspase activation in the cytoplasm, after 24 hrs. Notably, the Hill slope of the curve becomes dramatically steeper, and is well correlated with the order of the reaction, as shown in Figure 19, although notably, the correlation is not a direct 1:1, or linear one. At later times, however, a more linear relationship is observed and a close to 1:1 relationship between the Hill slope and the order of the reaction is observed.

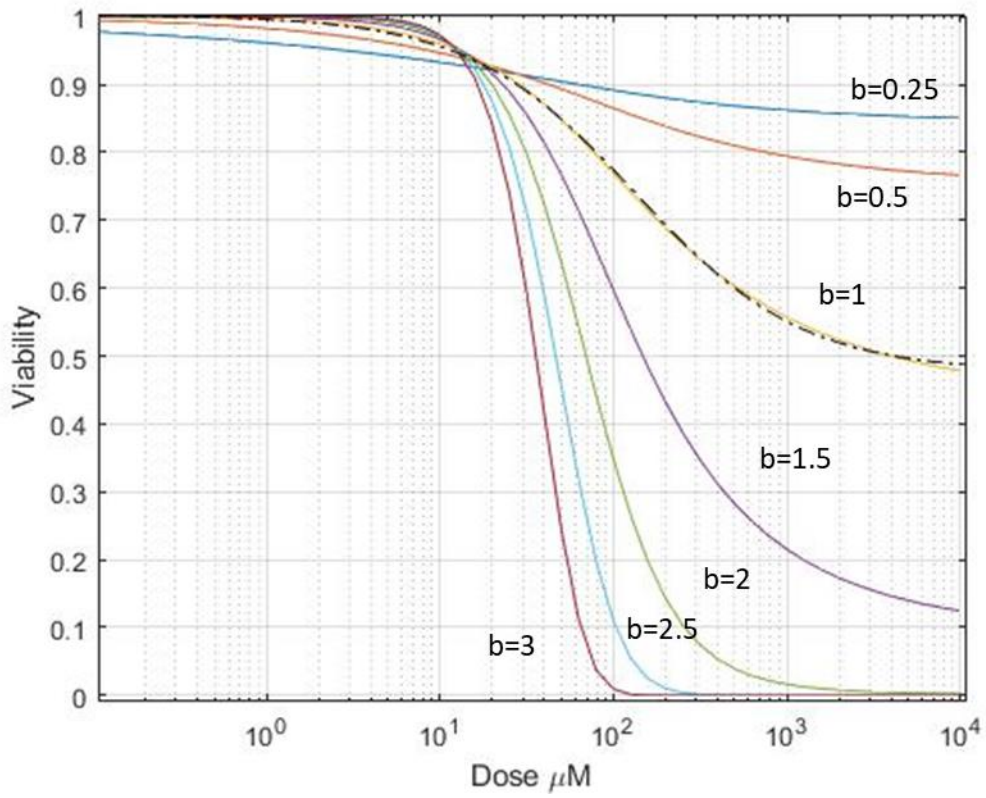

Figure 18: Dependence of the dose response curve on the stoichiometric parameter b of Equation 11. The dashed line shows a fit of the four parameter Hill equation to the simulated curve.

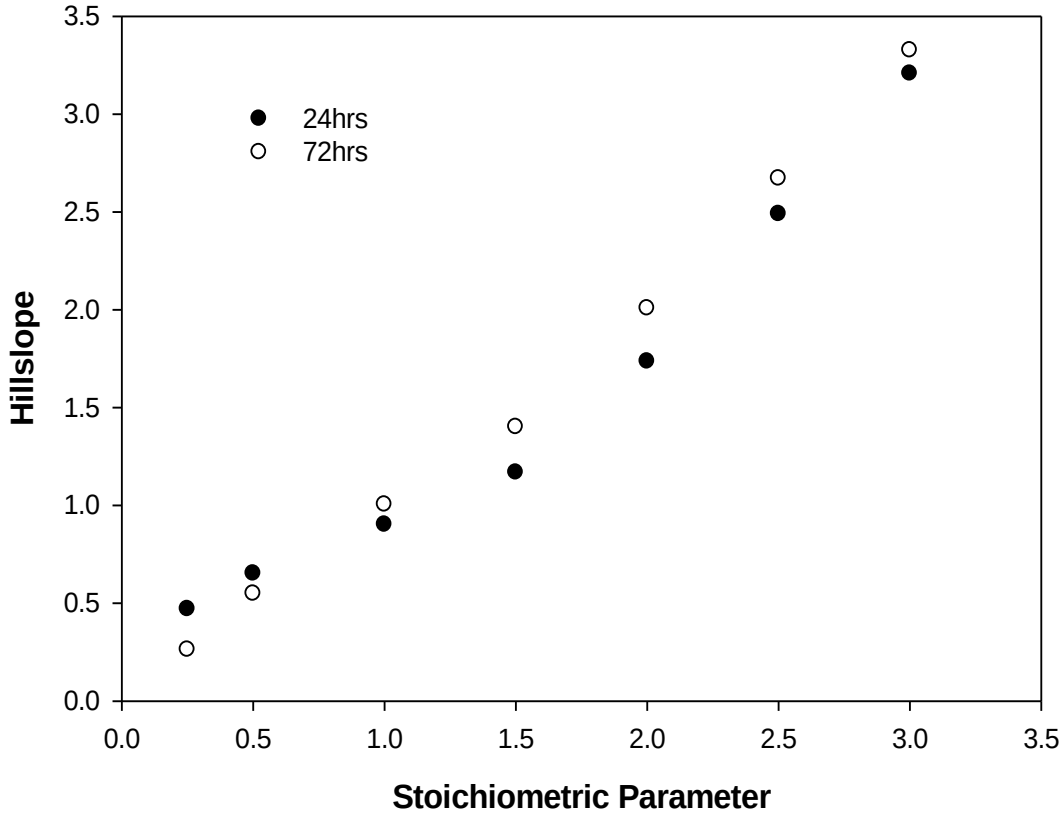

Figure 19: Correlation of Hill slope of the fitted dose response curve on the stoichiometric ratio of the cellular response.

The phenomenological rate equation approach can readily be extended to model the simultaneous action of one or more exogenous agents A and B, and to explore the characteristics of additive, synergistic and antagonistic behaviours. In a simple approach, the second agent B is endocytosed in parallel with agent B, at rate k_{endo2}, and contributes to the oxidative stress at a rate of k_{ROS2}. Equations 4 and 5 can be rewritten;

$$\frac{dN_{Source}}{dt} = -(N_{endo}.k_{ROS} - N_{endo2}.k_{ROS2}).N_{Source} \qquad \text{Equation (15)}$$

$$\frac{dN_{ROS}}{dt} = (N_{endo}.k_{ROS} - N_{endo2}.k_{ROS2}).N_{Source} - N_{GSH}.N_{ROS}.k_q \qquad \text{Equation (16)}$$

Both agents A and B contribute to the same intracellular response of generation of ROS and therefore to the subsequent cascade of cellular events. The dose dependent (D_A and D_B) behaviour is described by an isobologram, a representation first introduced by Loewe in 1927[37], and reviewed for example by Tallarida[38]. Figure 19 shows an example of an isobologram for agent A, using the parameters of Table 1, and agent B, with values of $k_{uptake2}$ = 5 x 10^{-7} $cell^{-1}hr^{-1}$ and k_{ROS2} = 5 x 10^{-4} $cell^{-1}hr^{-1}$. The straight line locus of IC_{50} for the combined doses is characteristic of an additive process, although it should be noted that the temporal profiles of the response curves for N_{ROS} and all subsequent responses in the cascade can change as a result of the different characteristic rates associated with the two agents, and can be used to differentiate their effects.

In the case, for example, where agent B also has the effect of increasing the cell membrane permeability and so the uptake rate of agent A, the effect can be simulated by;

$$k'_{uptake} = \left(1 \pm \frac{{D_B}^b}{a}\right).k_{uptake} \qquad \text{Equation (17)}$$

The positive sign increases the rate of uptake of agent A linearly, depending on the dose of agent B, whereas the negative sign decreases it. Alternatively, the stoichiometric ratio of the interaction can be different to 1, which can be simulated by the parameter *b*. The parameter *a* is included to modulate the degree of synergy/antagonism. Figure 19 shows examples of synergistic or antagonistic responses, in which k_{uptake} increases (*a*=50) or decreases (*a*=100) linearly with dose of agent B. Also shown is the response where the synergistic response is sublinearly dependent on the dose D_B, (*a*=1, *b*=0.25)

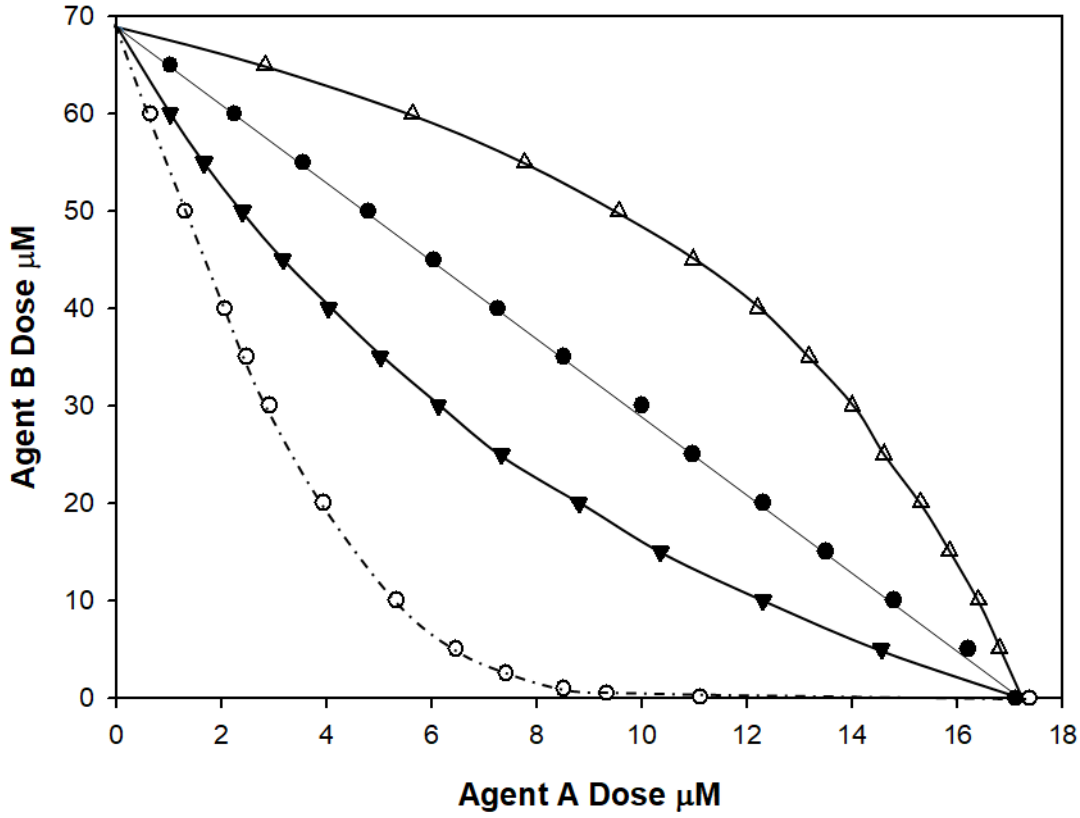

Figure 19: Isobolograme of two exogenous agents A and B, with respective IC_{50}s of 17 μM and 69 μM. Open Circles show the locus of a synergistic effect whereby the uptake rate of Agent A is dependent on $D_B^{0.25}$. Filled triangles show a synergistic effect in which the uptake rate of Agent A is increased linearly by Agent B, while the open triangles show an antagonistic effect in which the uptake rate of Agent A is decreased linearly by Agent B.

Discussion

The dose response curves of a cellular system to exposure to exogenous agents can be phenomenologically reproduced using a rate equation approach, which simulates the initial uptake of the agent, the initial cellular reactions and subsequent cascade of response

pathways. The dose response at any given time point faithfully reproduces the sigmoidal dependence commonly experimentally observed, often fitted analytically using a Hill equation, to yield a value of IC_{50} or EC_{50}. The simulation approach demonstrates, however, that the value of the median concentration is not uniquely characteristic of the agent, or the agent/cell line combination, and therefore the methodology of characterisation of cytotoxic responses according to dose response curves is somewhat questionable. Indeed, the analysis demonstrates that, despite the fact that it can be extremely sensitive to changes to certain individual characteristics of the system, the changes manifest in the dose response curve, describable by a four parameter Hill equation, are extremely non-specific in terms of the exposure or cellular parameters.

As shown by the analysis represented in Figure 5, the median response is dependent on the exposure time, as might be expected, and, although there is a correlation between the characteristics of the dose dependence and the exposure time, this correlation only holds once the exposure time is long in comparison to the timescale of the cellular events which impact the measured response. The measured dose response curve depends of course on the assay employed, as represented by Figure 13, and thus, at a given time-point, different assays can yield significantly different response curves, as they interrogate the respective response pathways at different stages of evolution of the pathway. The recommendation, therefore, is that cytotoxicological assays should be conducted for time periods of, as long as possible. Cellular response pathways can furthermore be sequential (Figures 12,13), parallel (Figure 16) and/or can give rise partial responses (Figure 17). These processes are not easily distinguishable by the dose dependent response, although their influence on the dose

response can be visualised using the numerical modelling approach based on rate equations to describe the dynamic evolution of the state of the system.

When visualised in the temporal domain, cytological responses are much more intuitively comprehensible. The sequence of events, from uptake to the final cytological outcome (e.g. apoptosis, necrosis), and importantly the influence of the properties of the external agent, can be distinguished from those of the properties of the test system, including cell line and assay, which can aid in understanding of the fundamental mechanisms of interaction, and thus guide strategies of, for example, drug design and predictive toxicology.

The rate of the initial uptake of the exogenous agent has, understandably, a critical impact on the cellular response, as shown in Figure 4. In the systematic study of a homologous series of PAMAM dendrimers in a range of human cell lines, when modelled using a similar rate equation approach[20], it was concluded that, while the uptake rate is largely independent of cell line, it is systematically dependent on particle size. This size dependent nanoparticle uptake rate was seen to extend to 50 nm aminated polystyrene (PS-NH_2) nanoparticles, in a similar study by Maher[39], in the same range of human cell lines. Both PAMAM dendrimers and PS-NH_2 nanoparticles have been seen to give rise to oxidative stress in the acidifying environment of the endosomes, by sequestering protons that are supplied by the v-ATPase (proton pump)[40]. It has been proposed that the initial wave of ROS may be produced via NADPH oxidase[41], an enzyme which produces superoxide anions (O_2^-) in phagosomes and endosomes[42], and thus may represents the source term of Equation (4), for this particular response pathway. The dose and time dependence of the generation of ROS is complex, but is well described as a function of particle dependent ROS generation rates, and cellular dependent parameters describing ROS source, antioxidant levels and ROS quenching rates.

Notably, for the homologous series of PAMAM generations 4-6, which have systematically increasing numbers of surface amino groups, the systematically varied oxidative response as well as resultant toxic response, was comprehensively described by variation of a single generation dependent parameter. The direct correlation of the exposure outcome on the structural properties of the external agent points towards clear QSARs. The rate equation approach is particularly suitable to visualisation of AOPs on a cellular level, in which QSARs govern the molecular initiating event (MIE) and the subsequent pathways are represented by the subsequent cascade of key events (KE) linked by key event relationships (KER), which, herein are the rate equations[23]. Indeed, recent work by Zgheib et al.[43] has explored the use of different routes towards quantification of AOPs, including a systems biology approach, similar to that employed here. The AOP approach is increasingly favoured for predictive toxicology to guide regulatory interventions[44]. The approach to quantitative analysis of the systems response is also key to metabolic flux analysis and fluxomics[45]. In the case, for example, of the chemotherapeutic agent, DOX, a dual pathway of mechanism of response has been described[46], whereby rapid transport to the nucleus/nucleoli of the cell results in binding with the RNA/DNA, a process which can similarly be considered a MIE, the limiting or source term being the number of RNA/DNA binding sites. Reversible reduction of DOX in the cytosol by several oxidoreductases to a semiquinone radical can also give rise to oxidative stress as a MIE[47,48], instigating an independent cascade of cellular events, which can be described by an independent or interlinked system of rate equations.

Notably, uptake of the external agent can occur via a number of different mechanisms, which can depend on the agent itself and the cell line used, and the subsequent cellular response can be substantially different. As an example, extending the series of poly (propylene imine)

dendrimers to generation 0-2, whereas the higher generations are seen to cause oxidative stress after endocytosis, the lower generations are seen to act as antioxidants, and the lack of evidence of endocytosis suggests a transition from active uptake of the larger higher generation dendrimers, to passive uptake of the smaller, lower generation[49]. Thus, an acellular assessment of the reactivity of an agonist is not sufficient to predict their cellular response[50].

The visualisation of the complex cellular mechanisms in the temporal domain provides a much more comprehensible picture of the response pathways, which can be represented mathematically by the system of rate equations. Figure 1 is of course a simplified model, but the system and the associated rate equations can be as complex, or as simple, as the challenge requires, and even extend to multi-omic pathway maps. Low dose, or early stage cellular responses can be key initial indicators of dysregulation of cellular machinery at later stages of the response pathway, more evident at higher exposure concentrations, and so monitoring such early stress and indeed adaptive responses can be important[51]. It should also be noted that the representation of Figure 1 does not include compartmentalised and inter-compartmentalised responses to describe the complete response of a cell. Increasingly, web-based resources are, however, available for such model building to describe the kinetic responses of cells in a systems biology approach, although they are not well adapted to dose responses[13,52]. Alternatives to colorometric based assays, such as impedance based cellular responses may provide real time monitoring of the state of the cellular system[53]. Notably, such a systems approach naturally lends itself to a broader approach to the responses systems on the organism level[12,19,54]. It should be noted that, as such models become increasingly complex and multiparametric, uncertainties of fitting to experimental data also increase, in

which case approaches such as parameter global sensitivity analysis (GSA)[19] could significantly enhance the robustness of the processes.

Conclusions

In vitro cytological dose response curves derive from a complex sequence of events, from cellular uptake of an exogenous agent, to internal interactions which trigger a cascade of response pathways resulting in a cellular outcome, which can be measured by a number of cytological assays in a number of different cell lines, at a number of seemingly arbitrary time-points. The four parameter curve is sensitive to any number of parameters en route, but the changes are not very specific to their causes, given the multitude of influencing factors. An understanding of these influencing factors can improve both the design and interpretation of dose response experiments. However, ultimately, monitoring the uptake processes and response pathways of the events, in a systems biology approach, provides the best understanding of their interdependencies, and can help extract independent properties of the exogenous agent, and the cellular system. Such an understanding can help to guide strategies for toxicology or preclinical drug screening, or even routes towards *in vitro* screening of patient sensitivities in a companion diagnostics approach[55].

Declaration of interests

The authors declare that they have no known competing financial interests or personal relationships that could have appeared to influence the work reported in this paper.

[1] European Union, “Legislation for the protection of animals used for scientific purposes - Environment - European Commission,” can be found under http://ec.europa.eu/environment/chemicals/lab_animals/legislation_en.htm, **n.d.**

[2] *Public Law 106-545 106th Congress An Act*, **n.d.**

[3] B. H. Mukherjee SP, Lyng FM, Garcia A, Davoren M, *Toxocology Appl. Pharmacol.* **2010**, *248*, 259–68.

[4] R. Gesztelyi, J. Zsuga, A. Kemeny-Beke, B. Varga, B. Juhasz, A. Tosaki, *Arch. Hist. Exact Sci.* **2012**, *66*, 427–438.

[5] O. US EPA, “Toxicology Testing in the 21st Century (Tox21),” can be found under https://www.epa.gov/chemical-research/toxicology-testing-21st-century-tox21, **n.d.**

[6] “TNRF Resources | National Center for Advancing Translational Sciences,” can be found under https://ncats.nih.gov/rnai/capabilities/resources#Robotic_Platform, **n.d.**

[7] M. D. Barratt, *Environ. Health Perspect.* **1998**, *106 Suppl 2*, 459–65.

[8] K. Kalani, D. K. Yadav, A. Singh, F. Khan, M. M. Godbole, S. K. Srivastava, *Curr. Top. Med. Chem.* **2014**, *14*, 1005–13.

[9] A. V. Hill, *J. Physiol.* **1910**, *40*, iv–vii.

[10] J. W. Black, P. Leff, *Proc. R. Soc. London. Ser. B, Biol. Sci.* **1983**, *220*, 141–62.

[11] A. Sorribas, B. Hernández-Bermejo, E. Vilaprinyo, R. Alves, *Biotechnol. Bioeng.* **2007**, *97*, 1259–1277.

[12] R. Steuer, B. H. Junker, R. Steuer, B. H. Junker, *Chem. Phys.* **2009**, *142*.

[13] Z. P. Gerdtzen, in *Genomics Syst. Biol. Mamm. Cell Cult.*, Springer Berlin Heidelberg, Berlin, Heidelberg, **2011**, pp. 71–108.

[14] A. Einstein, *Verhandlungen der Dtsch. Phys. Gesellschaft* **1916**, *18*, 318–323.

[15] W. Blau, H. Byrne, W. M. Dennis, J. M. Kelly, *Opt. Commun.* **1985**, *56*, 25–29.

[16] M. Miyazaki, S. Nakade, K. Iwanaga, K. Morimoto, M. Kakemi, *Drug Metab. Pharmacokinet.* **2003**, *18*, 350–357.

[17] S. M. Ryan, J. M. Frías, X. Wang, C. T. Sayers, D. M. Haddleton, D. J. Brayden, *J. Control. Release* **2011**, *149*, 126–132.

[18] A. Salvati, C. Åberg, T. dos Santos, J. Varela, P. Pinto, I. Lynch, K. A. Dawson, *Nanomedicine Nanotechnology, Biol. Med.* **2011**, *7*, 818–826.

[19] D. Dell'Orco, M. Lundqvist, T. Cedervall, S. Linse, *Nanomedicine Nanotechnology, Biol. Med.* **2012**, *8*, 1271–1281.

[20] M. A. Maher, P. C. Naha, S. P. Mukherjee, H. J. Byrne, *Toxicol. Vitr.* **2014**, *28*, 1449–1460.

[21] G. D. Souto, Z. Farhane, A. Casey, E. Efeoglu, J. McIntyre, H. J. Byrne, *Anal. Bioanal. Chem.* **2016**, *408*, 5443–5455.

[22] OECD, "OECD Quantitative Structure-Activity Relationships Project [(Q)SARs] - OECD," can be found under http://www.oecd.org/chemicalsafety/risk-assessment/oecdquantitativestructure-activityrelationshipsprojectqsars.htm, **n.d.**

[23] C. Wittwehr, H. Aladjov, G. Ankley, H. J. Byrne, J. de Knecht, E. Heinzle, G. Klambauer,

B. Landesmann, M. Luijten, C. MacKay, et al., *Toxicol. Sci.* **2017**, *155*, 326–336.

[24] S. P. Mukherjee, H. J. Byrne, *Nanomedicine Nanotechnology, Biol. Med.* **2013**, *9*, 202–211.

[25] S. P. Mukherjee, F. M. Lyng, A. Garcia, M. Davoren, H. J. Byrne, *Toxicol. Appl. Pharmacol.* **2010**, *248*, 259–268.

[26] Z. Farhane, F. Bonnier, O. Howe, A. Casey, H. J. Byrne, *J. Biophotonics* **2017**, *11*, e201700060.

[27] Z. Farhane, F. Bonnier, H. J. Byrne, *Anal. Bioanal. Chem.* **2017**, *409*, 1333–1346.

[28] P. C. Naha, S. P. Mukherjee, H. J. Byrne, *Int. J. Environ. Res. Public Health* **2018**, *15*, 338.

[29] S. P. Mukherjee, H. J. Byrne, *Nanomedicine Nanotechnology, Biol. Med.* **2013**, *9*, 202–211.

[30] K. E. Atkinson, J. Wiley, *AN INTRODUCTION TO NUMERICAL ANALYSIS Second Edition*, **1978**.

[31] M. A. Maher, P. C. Naha, S. P. Mukherjee, H. J. Byrne, *Toxicol. Vitr.* **2014**, *28*, 1449–1460.

[32] P. C. Naha, M. Davoren, F. M. Lyng, H. J. Byrne, *Toxicol. Appl. Pharmacol.* **2010**, *246*, 91–99.

[33] Z. Farhane, H. Nawaz, F. Bonnier, H. J. Byrne, *J. Biophotonics* **2018**, *11*, e201700258.

[34] B. I. Escher, P. A. Neale, D. L. Villeneuve, *Environ. Toxicol. Chem.* **2018**, *37*, 2273–2280.

[35] Z. Farhane, F. Bonnier, M. A. Maher, J. Bryant, A. Casey, H. J. Byrne, *J. Biophotonics* **2017**, *10*, 151–165.

[36] V. Pliska, *J. Recept. Signal Transduct.* **1999**, *19*, 597–629.

[37] S. Loewe, *Die Mischiarnei. Klin Wochenschr* **1927**, *6*, 1077–1085.

[38] R. J. Tallarida, *J. Pharmacol. Exp. Ther.* **1041**, *319*, DOI 10.1124/jpet.106.104117.

[39] M. A. Maher, Structure Activity Relationships Governing the Interaction of Nanoparticles with Human Cells – Predictive Models for Toxicology and Medical Applications, Dublin Institute of Technology, **2016**.

[40] A. E. Nel, L. Mädler, D. Velegol, T. Xia, E. M. V. Hoek, P. Somasundaran, F. Klaessig, V. Castranova, M. Thompson, *Nat. Mater.* **2009**, *8*, 543–557.

[41] T. Xia, M. Kovochich, J. Brant, M. Hotze, J. Sempf, T. Oberley, C. Sioutas, J. I. Yeh, M. R. Wiesner, A. E. Nel, *Nano Lett.* **2006**, *6*, 1794–1807.

[42] V. V Shuvaev, J. Han, K. J. Yu, S. Huang, B. J. Hawkins, M. Madesh, M. Nakada, V. R. Muzykantov, *FASEB J.* **2011**, *25*, 348–57.

[43] E. Zgheib, W. Gao, A. Limonciel, H. Aladjov, H. Yang, C. Tebby, G. Gayraud, P. Jennings, M. Sachana, J. B. Beltman, et al., *Comput. Toxicol.* **2019**, *11*, 1–13.

[44] *Unclassified ENV/JM/MONO(2013)6 JOINT MEETING OF THE CHEMICALS COMMITTEE AND THE WORKING PARTY ON CHEMICALS, PESTICIDES AND BIOTECHNOLOGY Revised Guidance Document on Developing and Assessing Adverse Outcome Pathways*, **2017**.

[45] D. Stewart, S. Dhungana, R. Clark, W. Pathmasiri, S. McRitchie, S. Sumner, *Syst. Biol. Toxicol. Environ. Heal.* **2015**, 57–83.

[46] "Doxorubicin Pathway (Cancer Cell), Pharmacodynamics Overview | PharmGKB," can be found under https://www.pharmgkb.org/pathway/PA165292163, **n.d.**

[47] G. Minotti, *Free Radic. Res. Commun.* **1989**, *7*, 143–8.

[48] G. Minotti, S. Recalcati, A. Mordente, G. Liberi, A. M. Calafiore, C. Mancuso, P. Preziosi, G. Cairo, *FASEB J.* **1998**, *12*, 541–52.

[49] H. Khalid, S. P. Mukherjee, L. O'Neill, H. J. Byrne, *J. Appl. Toxicol.* **2016**, *36*, 464–473.

[50] M. A. Maher, H. Khalid, H. J. Byrne, *Anal. Bioanal. Chem.* **2016**, *408*, 695–703.

[51] R. Judson, K. Houck, M. Martin, A. M. Richard, T. B. Knudsen, I. Shah, S. Little, J. Wambaugh, R. Woodrow Setzer, P. Kothya, et al., *Toxicol. Sci.* **2016**, *152*, 323–339.

[52] A. Funahashi, Y. Matsuoka, A. Jouraku, M. Morohashi, N. Kikuchi, H. Kitano, *Proc. IEEE* **2008**, *96*, 1254–1265.

[53] K. E. Garbison, B. A. Heinz, M. E. Lajiness, J. R. Weidner, G. S. Sittampalam, *Impedance-Based Technologies*, Eli Lilly & Company And The National Center For Advancing Translational Sciences, **2004**.

[54] H. Kitano, *Science (80-.).* **2002**, *295*, 1662–1664.

[55] "Overview of Companion Diagnostics in the Pharmaceutical Industry.," can be found under https://www.ddw-online.com/personalised-medicine/p92845-overview-of-companion-diagnostics-in-the-pharmaceutical-industry.html, **n.d.**